Construction and Building Materials 124 (2016) 1090–1099

Contents lists available at ScienceDirect

Construction and Building Materials

journal homepage: www.elsevier.com/locate/conbuildmat

Mode-specific damage identification method for reinforced concrete beams: Concept, theory and experiments

Liu Simeng [a,b,*], Zhang Liangliang [a], Chen Zengshun [c], Zhou Jianting [b], Zhu Chao [b]

[a] College of Civil Engineering, Chongqing University, Chongqing, PR China
[b] School of Civil Engineering, Chongqing Jiaotong University, Chongqing, PR China
[c] School of Engineering, The Hong Kong University of Science and Technology, Kowloon, Hong Kong

HIGHLIGHTS

- A strategy, developing mode-oriented damage identification methods, is suggested.
- The strategy possesses potential to greatly enhance effectiveness and specificity.
- The strategy was successfully validated in experiments on eight RC beams.

ARTICLE INFO

Article history:
Received 20 September 2015
Received in revised form 23 August 2016
Accepted 28 August 2016
Available online 3 September 2016

Keywords:
Damage identification (DI)
Structural health monitoring (SHM)
Mode-specific
Dominant failure mode
Reinforced concrete (RC) beam
Linearized deflection curve

ABSTRACT

Various structural failure modes exhibit great differences in occurrence probabilities, failure consequences and intrinsic characteristics, etc. Utilising these differences can enhance the effectiveness and efficiency of damage identification research, which has currently received little coverage. Therefore, a new idea, developing mode-specific damage detection methods, is suggested in the paper, with validation on beam structures. Firstly, structural behaviour was investigated from the perspective of stochastic traits and the structure design theory. It was concluded that developing damage detection methods for probabilistically dominant modes had potential to enhance the effectiveness of the identification significantly. Secondly, the strategy was applied to simply supported beams for the purpose of verification. When following the flexural mode, a major failure pattern of the beams, the structures demonstrated a very interesting feature – linearized deflection curves. Hence, damage severity and location indices were defined and an analytical model was built by quantifying the feature and then linking the indices to the curvature of the beams. Thirdly, experiments on reinforced concrete (RC) beams were conducted. The results showed that both the flexural mode and the characteristic of the linearized deflection curves were observed on all specimens; that there was a strong correlation between the damage severity index and the state of the defects on the beams; that the location indices corresponding to damaged and intact sections varied completely differently in quality and quantity. Thus, implementing the mode-specific strategy improves the specificity and efficiency of the damage identification dramatically.

1. Introduction

Civil structures usually need to operate for decades despite working loads, aging, environmental impacts and the related potential for damage accumulation. Therefore, evaluating the degree of deterioration of these constructions becomes increasingly important for both economic and safety purposes. Accordingly, in recent years, there has been enormous demand for techniques capable of detecting damage precisely, particularly in large structures such as long-span bridges. Structural health monitoring (SHM) technology is an effective solution to satisfy such demand [1]. In SHM systems, sensors are installed on structures to collect information [2] and Damage Identification (DI) techniques are employed to characterise structurally healthy and damaged states. So far, sensing technology has progressed greatly [3–5]. Hence, DI techniques are a key part of SHM research [6]. Although related studies have been conducted for decades [1,6–8], further investigations on damage detection are still a research priority.

* Corresponding author at: College of Civil Engineering, Chongqing University, Chongqing, PR China.
E-mail address: simengliu@163.com (S. Liu).

http://dx.doi.org/10.1016/j.conbuildmat.2016.08.133
0950-0618/

Generally speaking, the majority of current damage identification methods are usually suitable to all defects or failure modes of different structure types. The basic idea behind the methods, for instance the vibration-based techniques, is that model parameters such as frequencies, mode shapes, are functions of physical nature (mass, stiffness, damping); hence, the variations in the nature cause detectable changes in the modal parameters [9]; quantifying the measured changes is used to characterise their causes, namely damage. Following this philosophy, besides the vibration-based techniques [10–12], the artificial neural network-based technologies [13], the statistical pattern recognition-based methods [14] and the signal processing-based techniques [15,16], etc., were developed. Successful applications include the monitoring systems for the NASA's space shuttle [17], rotating machinery [18], wind turbines [19], offshore platforms [20], however, there are few on large-scale infrastructures such as long-span bridges [8,21,22]. For example, recently, Vardanega, et al. [23] pointed out that 'It remains difficult to get value from bridge monitoring'. Many excellent reviews [6–9,24] concerning the damage detection philosophy and progress is available. It is clear that the aforementioned concept cared little about the effect of distinctions among damage modes on the structural damage identification.

However, different types of damage vary dramatically in cause, evolution and consequence. Furthermore, changes of different nature and magnitude in structural properties and responses occur due to the complexity of different damage types. For example, Ji, et al. [25] found that damage (severe cracks or corrosion) altered the failure patterns of aged jacket platforms from a global yield in the intact state to a local tearing mode. Hence, to large-scale civil structures, identifying all kinds of defects with merely a single indicator or method is a really big challenge, even implausible [26]. Consequently, the distinctions among different defect/failure modes deserve more attention from the structural damage identification field.

Meanwhile, an in-depth understanding of failure modes is crucial for success in damage detection. Aktan, et al. [26,27] concluded that the characteristics of failure modes should be very well understood in order to identify damage or deterioration on bridges. Chase [28] and Das [29] asserted that the accurate estimates of system reliability and failure modes were essential for effective bridge management. Technically, among all possible modes, several occur more frequently [30] and they are probabilistically dominant. For example, a 10-truss structure was investigated by many researchers [31,32]. Feng, et al. [32] found that it could fail in thirty-four modes; however, the orders of magnitude of the failure probability of the first two modes were 10^{-4} and 10^{-5},respectively, whereas those of the rest were equal to or less than 10^{-12}. Namely, the structure mainly failed in the first two modes and the others were less important. In this case, once the two modes instead of all thirty-four ones were covered by corresponding mode-specific damage identification techniques, the safety of the structure would be enhanced significantly. Furthermore, as is analysed later, compared with the universal DI investigations, studying DI methods for the probabilistically dominant modes is more deterministic and easier. In conclusion, implementing mode-specific damage identification research is inherently essential.

This study suggests a mode-specific damage identification strategy verified by tests on reinforced concrete beams. The paper is structured as follows. In Section 2, a main failure mode of simply supported beams, the flexural mode, is analysed theoretically; a characteristic termed the deflection curve linearization is uncovered; a direct relation between the damage severity and the characteristic is established. In Section 3, a functional form of the deflection curves of damaged beams is deduced based on the finite element theory; the damage detection problem is transformed into quantifying the difference between the deflection curve and its secant, utilizing the Fourier series approach; the damage location and severity indices are defined based on the mathematic interpretation of the difference, using the Difference Method and the previously obtained Fourier coefficients. In Sections 4 and 5, experiments on RC beams are investigated; the flexural mode, the deflection curve linearization and the performance of the two indices are examined completely. Finally, the strategy, conducting the mode-specific damage detection research, is discussed from the perspective of theoretical necessity and engineering practice.

2. The flexural failure mode of RC beams and its feature

2.1. The flexural mode, a dominant failure mode of RC beams

The flexural failure mode is stochastically dominant in RC structures [33–35], thanks to the excellent performance of structures which fail in the mode. In an RC beam, the flexural failure mode can be characterised by two features [33,36]. Firstly, tensile reinforcement in a certain section yields and part of concrete in compression is crushed almost simultaneously when failure occurs. Secondly, the beam exhibits enormous deformations during failure. Two corresponding factors account for the overwhelming predominance of the mode. The first is to fully utilize the reinforcement and concrete strength. The second is to give engineers an early warning and opportunity to save the structure and avoid the loss of life and property. In fact, since these traits have been clearly understood throughout the civil engineering community, engineers are required to design structures to fail in this mode in major RC design specifications [33,35,37,38]. Namely, most RC structures have mode-preference nature when being designed. Therefore, it is inherently inevitable to employ the flexural mode-specific techniques to identify their damage. Additionally, the strategy is also applicable to other structures.

Technically, the predominance of the flexural mode was demonstrated clearly and completely in the experiments detailed in Sections. 4 and 5. Firstly, in the theoretical estimation, for example, for loads of 50 kN, the failure probability of the flexural mode was 0.5091, whereas those of the others were equal to or less than 9.1291×10^{-6}. Namely, the probability of the former was five orders of magnitude greater than those of the others. Secondly, in situ, all specimens failed in the flexural mode.

Randomness also plays an important role, which results from stochastic factors, for instance, construction errors and the deviations of material properties from those assigned in design. For example, the beams in the following experiments were designed such that they theoretically failed in the flexural mode; however, the precise breakage position was unknown before a test.

2.2. The behaviour of RC beams failed in the flexural mode

In this section, the behaviour of a beam failed in the flexural mode is analysed in order to establish the relation between the damage severity and curvature of the structure. In Panel a) of Fig. 1, a beam subject to a concentrated load P at X_p has a major crack within the region $[X_{CL}, X_{CR}]$. The damaged segment is simulated by reducing its properties, such as stiffness and capacity [39]. Assume that, except for the damaged segment, the other parts of the beam behave elastically [40] and the bearing capacity of the cracked section is reached when the damage starts to worsen.

There is a direct relation between the damage severity and the curvature of the residual beam segments. Take the left-hand part depicted in Fig. 1 as an example. The flexural moment is in equilibrium near the cracked segment; the rotation at both sides of Section N is compatible, whereas the curvature is discontinuous

$$M_{NL} \equiv M_{NR}, \theta_{NL} \equiv \theta_{NR} \quad (1)$$

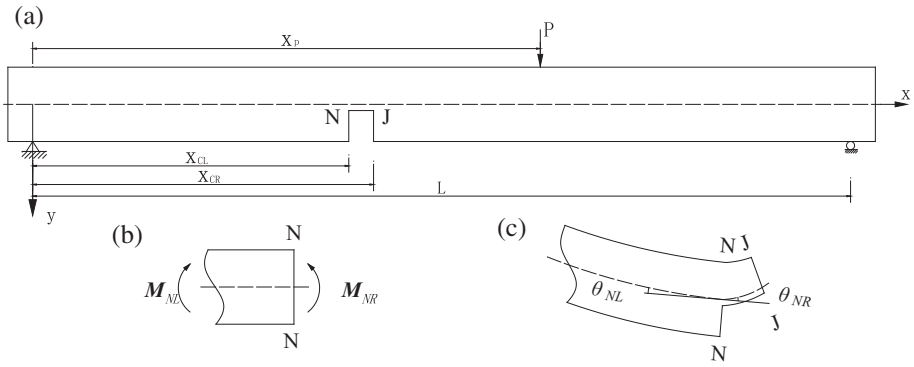

Fig. 1. The theoretical model of a cracked beam: a) the cracked beam [39]; b) the bending moment equilibrium existing at both sides of the crack section; c) the deformations near the cracked segment.

$$D_L''(x_N) \neq D_R''(x_N) \tag{2}$$

Here, x_N equals x_{CL}; $M_{NL}, M_{NR}, \theta_{NL}$ and θ_{NR} are the flexural bending moment and the rotating angles at the left and right sides of Section N; $D_L''(x_N)$ and $D_R''(x_N)$ are the curvatures occurring at both sides of Section N. As assumed previously, the left-hand part of the beam is an elastic segment and therefore the relation between the flexural moment M_{NL} and the corresponding curvature $D_L''(x_N)$ is

$$M_{NL} \cong EI * D_L''(x_N) \tag{3}$$

where EI is the bending stiffness of a section which is uniform throughout the entire beam in this study. Consider Eqs. (1) and (3), and therefore M_{NR} is

$$M_{NR} = M_{NL} = EI * D_L''(x_N) \tag{4}$$

Since Section N reaches its current capacity, the damaged extent γ is defined as the ratio of the residual capacity to its original magnitude

$$\gamma = \frac{M_{NR}}{M_{Nu}} = \frac{EI}{M_{uN}} * D_L''(x_N) = W_L * D_L''(x_N) \tag{5}$$

γ varies from 1 (intact) to 0 (failed); M_{Nu} is the flexural capacity of Section N in the pristine state; M_{NR} is the residual capacity of Section N and also equals the bending moment produced by load P; W_L is a constant related to the properties of the beam segment

$$W_L = \frac{EI}{M_{Nu}} = \frac{EI}{P_{max} * x_p}$$

where P_{max} is the maximum load that the beam can bear; x_p is the arm of P. Eq. (5) shows that the damage severity is proportional to the curvature occurring at the end of a residual part.

When the load P is small, since the major crack has not occurred or is developed very slightly, there is equilibrium between the load P and the inner force

$$M_N = P_{Lower} * x_p = EI * D''(x_N) \tag{6}$$

where P_{Lower} is of such a small magnitude that the beam is almost intact; M_N and $D''(x_N)$ are the corresponding bending moment and curvature. Therefore,

$$EI = \frac{P_{Lower} * x_p}{D''(x_N)} \tag{7}$$

Substituting Eq. (7) into Eq. (5) yields

$$\gamma = \frac{EI * D''(x_{NL})}{P_{max} * x_p} = \frac{P_{Lower} * D_L''(x_N)}{P_{max} * D''(x_N)} = \frac{P_{Lower}}{P_{max} * D''(x_N)} * D_L''(x_N) = L_W * D_L''(x_N) \tag{8}$$

Compared with Eq. (5), Eq. (8) is more convenient to utilise in a test since all involved quantities are experimentally measurable.

2.3. The deflection curve linearization of RC beams failed in the flexural mode

The deflection curve linearization refers to a feature, a linearized deflection curve of the beams, which appears when the damage is worsening. It is a consequence of the flexural failure mode.

Re-write Eq. (5) as follow

$$M(x_N) = M_{NL} = M_{NR} = \gamma * M_{Nu} \tag{9}$$

where $M(x_N)$ is the bending moment at Section N. Eq. (9) implies that the bending moment on the whole beam decreases when the damage worsens ($\gamma \to 0$). Hence, the elastic deflections of the beam, $D_e(x)$, also decrease, because, for example, the deflection of the left segment is

$$D_e(x) = \int\int \frac{M(t)}{EI} dtdt = \int\int \frac{M(x_N)}{EI * x_N} tdtdt = \gamma * \left[\int_0^x \int_0^x \frac{t}{W_L * x_N} dtdt + f(x) \right] = \gamma * \left[\frac{x^3}{6W_L * x_N} + f(x) \right]$$

where $f(x)$ is a function related to the boundary conditions.

More importantly, there is a rigid displacement component on each segment which increases during failure ($\gamma \to 0$). As shown in Eq. (2), the curvature distribution at both sides of Section N is discontinuous. With the development of the damage, the discontinuity results in a tremendous curvature jump. Consequently, as shown in Fig. 2, a rigid rotation, θ_{NLr}, occurs on the left segment. θ_{NLr} triggers the rotation of the segment about its support, a rigid displacement which contributes to a considerably large part of the segmental deformation; what's more, the rigid displacement is distributed linearly along the segment and increases dramatically with the damage. These two parts – the elastic deflection and rigid displacement, facilitate Section N to satisfy the compatibility of rotation (the second equation in Eq. (1)). Since the former decreases and the later increases greatly with the damage, the geometrical shape of each segment is being linearized when the damage increases ($\gamma \to 0$). Additionally, to the right portion of the beam, the presence of load P gives a bigger weight to the elastic deflection; however, the nature of the problem remains identical. In conclusion, the deflection shapes of both segments turn from curved to straight and tend to coincide with their secants; this feature reflects the progress of the damage.

So far, a unique characteristic which occurs when the structure fails in the flexural mode is extracted. Furthermore, as shown below, the difference between the deflection curve of the beam

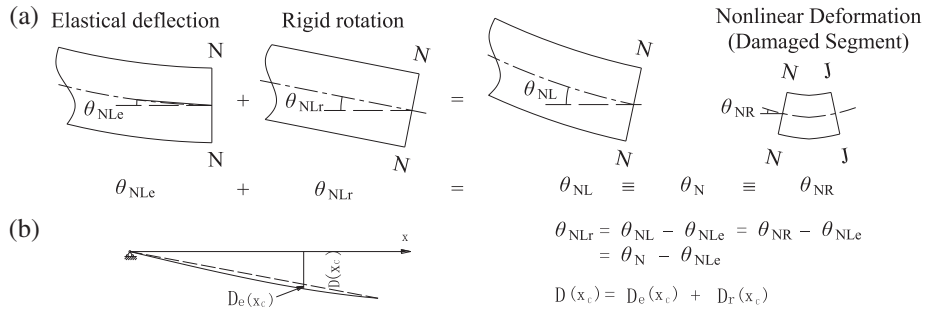

Fig. 2. The deformation near the cracked segment and the left-side segment of the beam: a) the compatibility of the deformation occurring at both sides of Section *N*; b) the combination of the elastic and rigid deformations of the segment.

and its secant relates to the damage severity; the position of a sharp turning on the curve helps to locate the damage.

3. The flexural mode-specific damage identification method

In this section, mathematically formulating the deflection curve linearization is used to identify the damage on beams that follow the flexural mode. In the following, the functional form of deflected beam curves is established. The mathematical implication of the deflection curve linearization is discussed, and the Fourier series approach is introduced for characterisation. Finally, damage severity and location indices are defined.

3.1. The function form of deflection curves of damaged beams

In order to estimate the damage severity by quantifying the difference between a deflection curve and its secant, the first target is to determine the functional form of both geometrical objects. As is known, the secant is a line; hence, the key is the determination of the deflection curve function form.

In finite element (FE) theory, the deformation of a two-dimension frame element is estimated based on its nodal displacements

$$D(x) = \varphi_1(x) * v_1 + \varphi_2(x) * v_2 + \varphi_3(x) * v_3 + \varphi_4(x) * v_4$$

where $D(x)$ is the deflection at x. As shown in Panel b) and c) in Fig. 3, v_i and $\varphi_i(x)$ ($i = 1, 2, 3$ or 4) are the nodal elastic displacement and shape function of the ith degree of freedom (DOF), respectively. A common form of $\varphi_i(x)$ is given in, for example, reference [41]

$$\varphi_1(x) = 1 - 3\left(\frac{x}{L_0}\right)^2 + 2\left(\frac{x}{L_0}\right)^3 = 1 - \varphi_2(x)$$

where L_0 is the elemental length. It is clear that the elastic deflection at x and the entire curve of the structure are uniquely determined by all the nodal displacements.

For the remaining segments, the damaged section serves as one of two ends and the other is the support. Meanwhile, consider the boundary conditions, i.e. for the left-hand segment $v_1 = 0$ and for the right-hand one $v_2 = 0$, and reduce the function of either segment as: for the left-hand portion

$$D(x) = \varphi_2(x) * v_2 + \varphi_3(x) * v_3 + \varphi_4(x) * v_4$$

and for the right-hand portion

$$D(x) = \varphi_1(x) * v_1 + \varphi_3(x) * v_3 + \varphi_4(x) * v_4$$

Eventually, consider the rigid deformation discussed in Section 2.3 which is a linear term and then further simplify both as

$$D(x) = Ax^3 + Bx^2 + Cx + D \tag{10}$$

where x is the abscissa of a section of interest and belongs to [0,xCL) or (xCR,L]; A, B, C and D are coefficients which vary with the damage. In conclusion, the deflection curve function of a residual segment is a cubic polynomial.

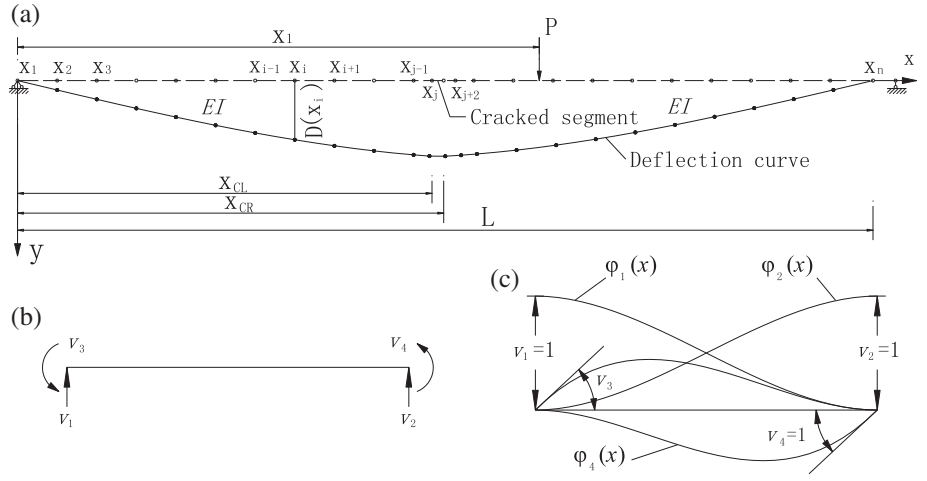

Fig. 3. The deflection curve of a damaged simply supported beam: a) a deflection curve; b) a two-dimension frame element; c) the shape functions of the element.

3.2. The formulation of the deflection curve linearization

In order to quantify the damage severity, the second target is to mathematically characterise the difference between a curve and its secant. From the mathematical perspective, the deflection curve linearization may be interpreted as follows: if a curve is being linearized, the difference between it and its secant is narrowing. Therefore, the damage diagnostic problem can be transformed into that of quantifying the difference mathematically. Hence, the Fourier series approach is hereafter introduced. The primary idea is that the deflection curve and its secant functions are expressed in a Fourier series form and then the difference is quantified by comparing the Fourier coefficients.

The main procedure is detailed as follows. Firstly, obtain the functional expressions of the deflection curve and its secant in a mathematical or experimental way. The function of the secant, $S(x)$, corresponding to Eq. (10) is

$$S(x) = \frac{delB - delE}{x_b - x_e} * (x - x_b) + delB, \quad 0 \leqslant x_b \leqslant x \leqslant x_e \leqslant L$$

where x_b, x_e are the x coordinates of both ends of the beam segment; $delB = D(x_b)$ and $delE = D(x_e)$ are the deflections at x_b and x_e. Secondly, both functions are periodically extended with a method such as the odd/even/periodical prolongation. Eq. (10) can be oddly extended as

$$D(x) = \begin{cases} Ax^3 + Bx^2 + Cx + D & \text{if } x \in (nL, (n+1)L] \\ 0 & \text{if } x = nL (n = 1, 2, 3, \cdots) \\ Ax^3 - Bx^2 + Cx - D & \text{if } x \in (nL, (n-1)L] \end{cases}$$

Thirdly, the two extended functions are expressed in a Fourier series form, which produces two series of Fourier coefficients. For example, Eq. (10) can be oddly prolonged and then expressed in the Fourier series form as

$$P(x) = \sum_{i=0}^{n} b_n \sin\frac{n\pi x}{L} \tag{11}$$

where $P(x)$ is $D(x)$ or $S(x)$; $b_n (\mathrm{n} = 1, 2, 3, \cdots)$ are Fourier coefficients

$$b_n = \frac{2}{L}\int_0^L P(x)\sin\frac{n\pi x}{L}dx (n = 1, 2, 3, \cdots) \tag{12}$$

Hence, the two sets of coefficients form two vectors

$$\alpha_D = [b_{D1}, b_{D2}, b_{D3}, \cdots] \text{ and } \beta_U = [b_{U1}, b_{U2}, b_{U3}, \cdots]$$

where α_D is a vector, called a Fourier coefficient vector, whose components, b_{D1}, b_{D2}, b_{D3}, are associated with the curve; is also a vector and its components, b_{U1}, b_{U2}, b_{U3}, are related to the secant. Finally, the damage severity can be quantified precisely by comparing the two vectors.

3.3. The damage extent index

In principle, if two geometrical objects tend to coincide with each other, the angle between their Fourier coefficient vectors, α_D and β_U, should approach zero. Therefore, the damage extent index, termed the angle index, is defined as

$$L_A = \mathrm{acos}\left(\frac{\{\alpha_D \cdot \beta_U\}}{|\alpha_D| * |\beta_U|}\right) \tag{13}$$

where L_A is the angle index; $\{\alpha_D \cdot \beta_U\}$ is the dot product of Vectors α_D and β_U; the operator $|\alpha_D|$ gives the absolute magnitude, i.e. the length, of vector α_D; $acos(\cdot)$ is the anti-cosine function. According to its mathematical meaning, L_A should tend to a value of zero, with increasing damage ($\gamma \to 0$).

3.4. The damage location index

Locating damage is based on the fact that if the curvature distribution is discontinuous (Eq. (2)), a turning appears on the curve; furthermore, the turning point is just the location of the damage. The location index DL_i is termed the slope index and defined as

$$DL_i = \frac{K_{i1}}{K_{i2}} = \frac{\tan\alpha}{tan\beta} = \frac{D'_L(x_i)}{D'_R(x_i)} = \frac{\int_{x_{i-1}}^{x_i} D''(x)dx}{\int_{x_i}^{x_{i+1}} D''(x)dx} \tag{14}$$

where DL_i is the slope index used to check whether the damage occurs at Node i; as shown in Fig. 4, $K_{i1} = \tan\alpha$ and $K_{i2} = \tan\beta$ refer to the slopes of the segments at both sides of node i, respectively

$$K_{i1} = \frac{\Delta D_{i,i-1}}{\Delta x_{i,i-1}} = \frac{D(x_i) - D(x_{i-1})}{x_i - x_{i-1}} K_{i2} = \frac{\Delta D_{i+1,i}}{\Delta x_{i+1,i}} = \frac{D(x_{i+1}) - D(x_i)}{x_{i+1} - x_i} \tag{15}$$

where x_{i-1}, x_i and x_{i+1} are the x-coordinate of Node $i-1$, i and $i+1$; $D(x_{i-1})$, $D(x_i)$ and $D(x_{i+1})$ are the displacement values at these nodes; $\Delta x_{i,i-1}$ and $\Delta x_{i+1,i}$ are the coordinate increments between Node $i-1$ and i, i and $i+1$; $\Delta D_{i,i-1}$ and $\Delta D_{i+1,i}$ are the displacement increments between the two pairs of nodes.

In Fig. 4, the varying patterns of the slope indices in three situations are depicted. In Panel a), the specimen is pristine and the slopes of two neighbouring segments are different; hence, the value of DL_i is far greater than a value of unity. In Panel b), the beam is approaching failure but the hinge is not formed at Node j; hence, DL_j is approaching 1.0. In Panel c), a hinge is being developed at Node k; therefore, the curve sharply turns here and the index value is negative. Note that the slope index at the mid-span is singular in theory because the values of K_{j1} and K_{j2} are near-zero; however, in practice, if the hinge is formed at the mid-span, the variation of the index is similar to that of Node k in Panel c); otherwise, the slope index follows the pattern of Node j in Panel b). In conclusion, the location of the hinge, namely the damage, can be determined precisely by monitoring the slope indices at all measuring points.

4. Experiments on RC beams

Experiments on eight RC beams were carried out to verify the previously discussed output. The mechanical properties of the materials involved are shown in Table 1. The symbol E denotes the elasticity modulus of steel or concrete. For concrete, f_c and f_t denotes the compression strength and tensile strength, respectively; for steel bars, f_c and f_t refer to the yield strength in compression and in tension. The diameters of all reinforcement are listed in the "D(mm)"column. The "Notation" column names all steel bars. The "State" column shows the states of the steel bars, in compression or tension, when the beams are subjected to loading. The design details (the cross sections and reinforcement configuration, etc.) are presented in Fig. 5. The total beam length was 3.5 m, whereas the clear span, the distance between two supports, was 3.3 m.

Specimens were subjected to two concentrated forces with the same magnitude and in an identical direction. The horizontal distance between the force and the nearest support was 1.1 m. Namely, the loading positions were within the regions where the stirrups were installed. This was crucially important to lead the structures to fail in the flexural mode.

Deflections, strains and cracks were measured. Thirteen transducers were equally spaced along the longitudinal axis of a beam to capture its precise deflections. Steel strain gages were applied on all the longitudinal bars on the cross sections of the mid-span, one- and three-quarters of the clear span. Concrete gages were also employed to measure strain on one side face of the mid-span. All cracks were marked and the width and length of typical cracks

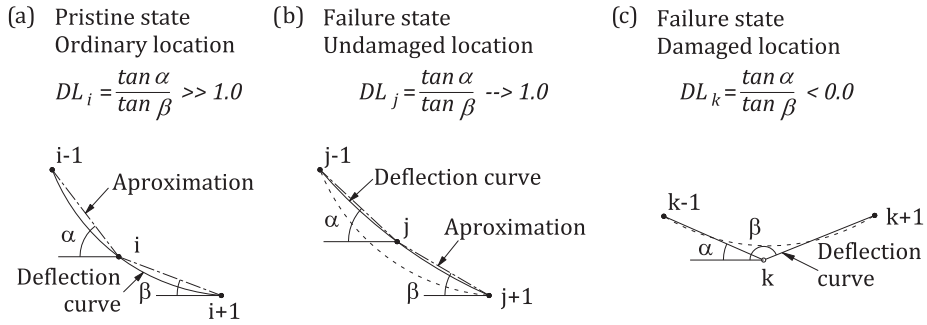

Fig. 4. The slope indices DL_i in three situations (a practical deflection curve, the solid line; an approximation, the dash-dotted line; the curve in the intact state, the dashed line).

Table 1
The mechanical properties of the materials involved in the experiments.

Material type	D (mm)	E (MPa)	f_t (MPa)	f_c (MPa)	Notation	State
Concrete	\	3.0E+4	2.01	20.1	\	\
Steel bars	16	2.0E+5	335	335	N_1	Tension
	8	2.1E+5	235	235	N_2	Compression
	8	2.1E+5	235	235	N_3	Shear

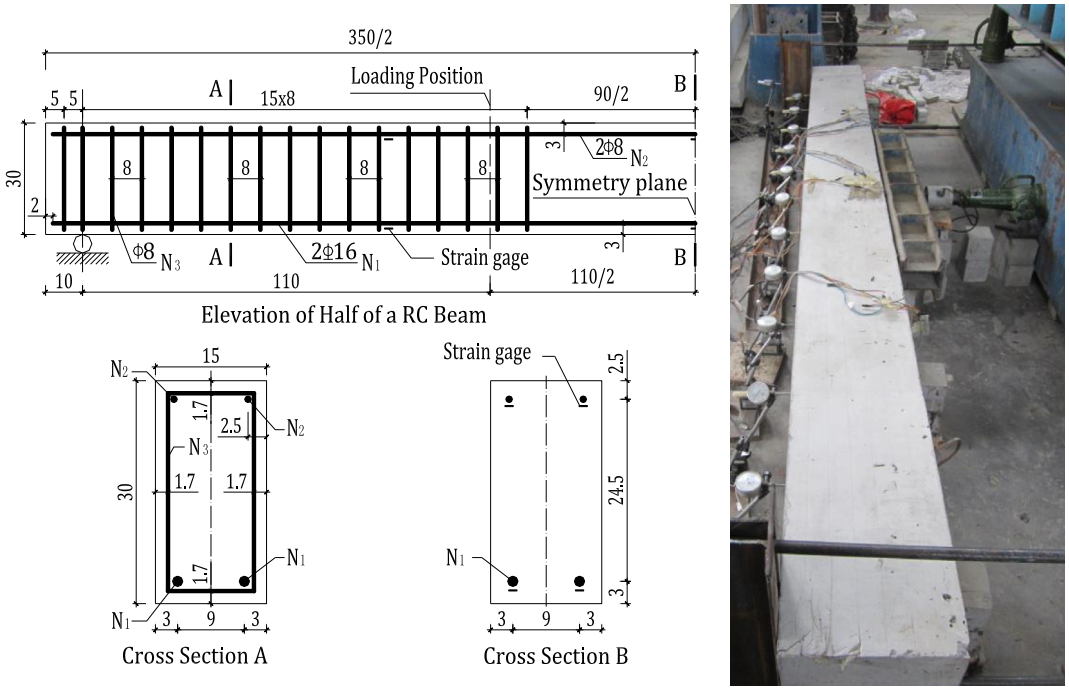

Fig. 5. Design details of an RC beam (Unit in cm) and a specimen in situ (right).

were recorded. Some of the measurement devices are also shown in Fig. 5.

5. Discussion

The failure mode and its feature of the specimens and the effectiveness of the location index and the severity index are investigated carefully below. As assumed previously, the damage discussed here refers to what occurred in the hinged or heavily damaged segment rather than tiny cracks. Note that the data from Specimen 6 instead of all beams are highlights in the following discussion due to limited space available here.

5.1. The failure mode and the feature observed on specimens

The observations from the specimens match very well with the theoretical prediction in Sections 2.2 and 2.3 regarding the flexural failure mode. On Specimen 6, when the load $2^*P = 90$ kN, the tensile reinforcement yielded suddenly; after a while (the peak load, 93 kN), on the same section, the concrete strain on the top exceeded the ultimate strain limit and resulted in concrete crashing; the beam stiffness decreased enormously and the deflections increased tremendously as shown in Fig. 8. The beam reached its capacity and the hinge was formed completely as shown in Fig. 6. In the lower panel of Fig. 6, in the damaged area, the upper part of the concrete is crushed; the lower part and the bars inside

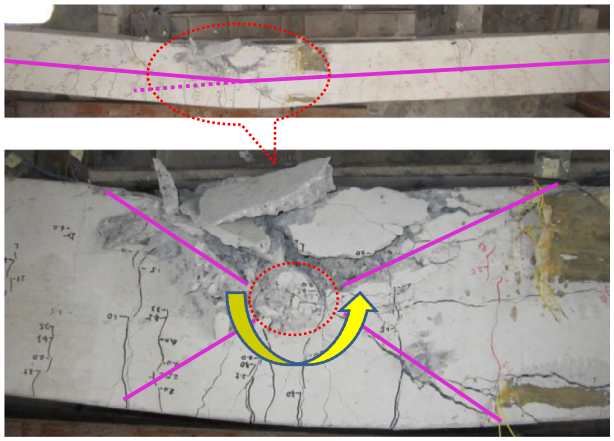

Fig. 6. Beam 6 in the failure state (the upper) and the corresponding damaged zone (a hinge).

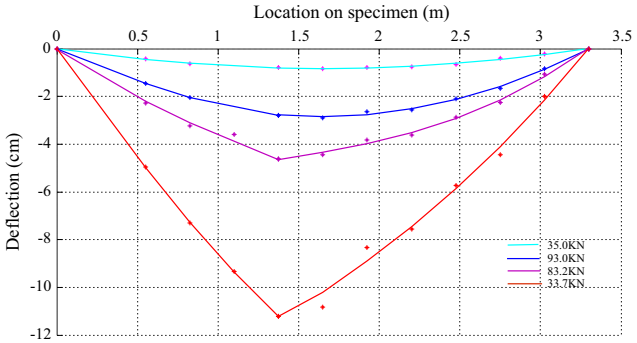

Fig. 8. The deflection curves of Specimen 6 under four load levels: 1) 35.0 kN, a slightly damaged state; 2) 93.0 kN (the peak load), forming a hinge; 3) 83.2 kN, full formation of the hinge; 4) 33.7 kN, the state of complete failure.

are tensioned to failure; the concrete hinge facilitates the segmental rotation about the centre of the damaged zone.

Randomness, an important aspect of failure modes, indeed played a critical role although all involved factors were handled as precisely as possible. The hinge distribution on all specimens reflects the feature. In Fig. 7, the damage location is represented by the x coordinate of the transducer adjacent to the damage on each beam. The distribution of hinges is characterised as below. Firstly, all hinges appear in the region between the two loads P, namely on the pure bending segments which also have the largest flexural moment and the highest failure probability. Secondly, they are almost evenly spread, which reflects the fact that all sections within the region are of identical failure probability. In conclusion, all specimens fail in the flexural mode.

The deflection curve linearization characteristic was observed on all beams. Fig. 8 shows the deflection curves of Beam 6 in four stages. When there was slight damage, such as tiny cracks, the curve (the uppermost one) was nearly of a polynomial shape. With the development of the damage, the curve was gradually divided into two portions by the heavily cracked segment at x = 1.375 and both portions became straighter. Once the hinge was formed fully, the shape of the beam axis (the lowermost curve) consisted of two lines, as also shown in the upper panel in Fig. 6. In conclusion, with the worsening of the damage, the linearizing tendency of the deflection curve became clearer.

The failure characteristics described above clearly show that the RC beams fail in the flexural mode. These results prove that the foundation of this research and the DI technique developed here is valid.

5.2. The effectiveness of the damaged extent index

Before analysis of the experimental data, some details need explaining. Consider the loading condition shown in Fig. 7. Eq. (5) becomes

$$M_{NR} = \gamma \cdot M_{Nu} = 1.1P$$

$$\gamma = \frac{1.1}{M_{Nu}} \cdot P$$

where, as shown in Fig. 7, the constant 1.1 refers to the arm of load P. The above equation shows that the extent of the damage is proportional to P during the formation of the hinge. Namely, P can serve as a direct reference to the damage extent. Hence, the load history is embedded in the following plots. Meanwhile, the effectiveness and validation of the indices are examined by checking the correlation between P and the indices. Additionally, the sequence of the loading steps is introduced as the horizontal axis of these plots. Note that the first ten Fourier coefficients were involved in the calculation of L_A.

The variation of the damage extent index L_A during the test on Beam 6 is demonstrated in Fig. 9. The procedure was characterised by three-phase features. In the first phase, the load P increased from 35.0 kN to 90.0 kN, and the value of L_A fluctuated around a value of 0.09. The load-deflections of the mid-span (Panel (b)) provides more insight into what happened during this stage. As shown in Panel (b), the slope of the curve is nearly constant from point B' to C'. From the point of view of the concrete structural theory, this means that the beam stiffness was nearly invariable [34]. Namely, both the structure and damage states were very steady – neither increasing nor decreasing significantly. This gives a full explanation of the tiny fluctuations around 0.09. The values of the first two points are too small; this results from measurement errors, because the beam only deflected slightly at the beginning of the test. The second phase started when P = 93.0 kN (the peak load) and ended when P = 55.0 kN; the values of L_A decreased from 0.09 to 0.03. Even more importantly, the variation coincides exactly with the decrement of P. Further analysis found that there is another three-stage procedure in this phase; L_A correlates closely with P in every stage. At the end of the test, the beam failed completely, and the index varied slightly again. In conclusion, there is a strong correlation between the damaged state and the index value.

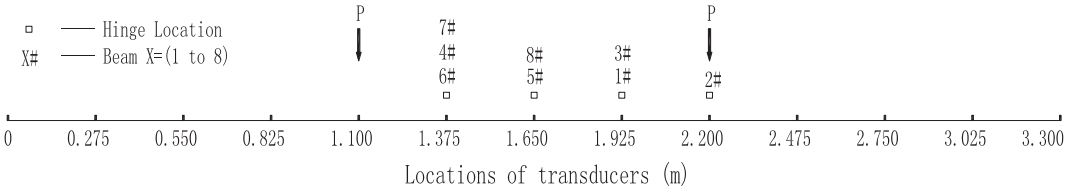

Fig. 7. The hinge distribution on all specimens.

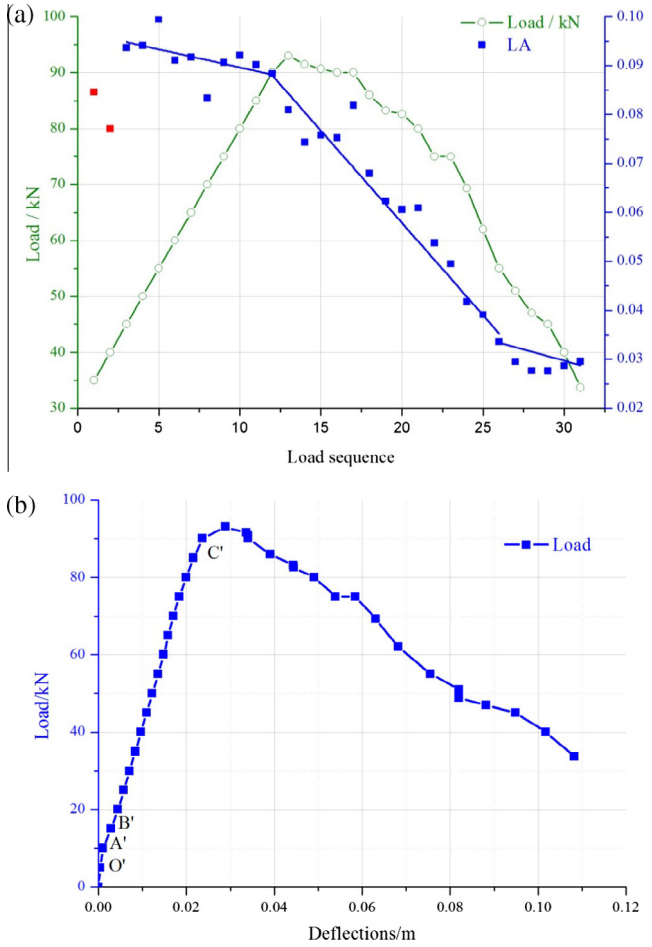

Fig. 9. The variation of the severity index L_A and the load-deflection relation during testing on Specimen 6.

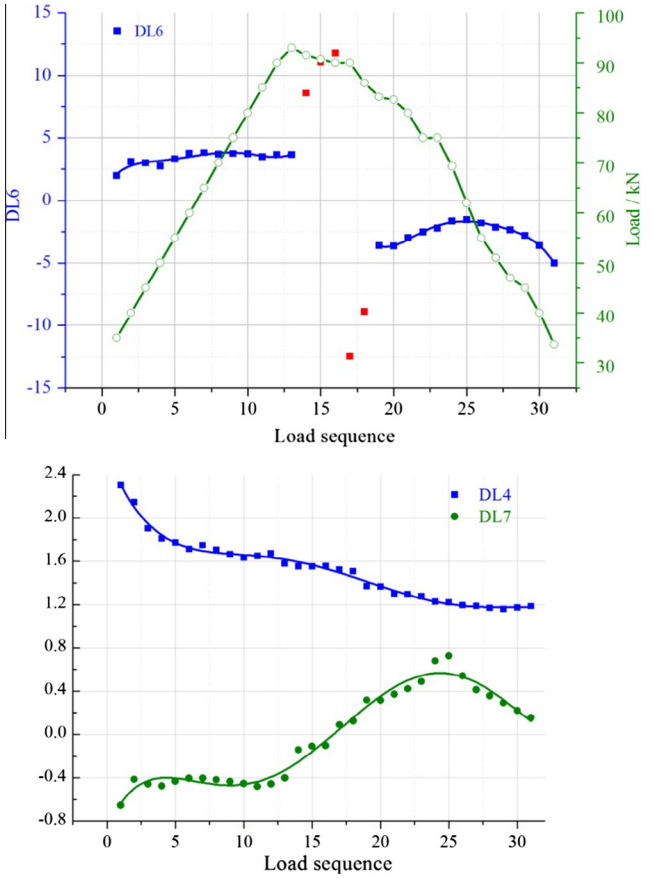

Fig. 10. The variations of the location indices DL_i at three cross sections: DL_6, the hinged section; DL_4, a common section; DL_7, the mid-span.

5.3. The verification of the damage location index

The data from sections 3, 4, 6, 7 and 8 were evaluated to completely investigate the performance of the location index. Accordingly, three indices, DL_4, DL_6 and DL_7, were analysed. DL_6 was selected since the hinge was near the sixth transducer as shown in Fig. 10. DL_7 was involved in order to study the index performance at a special location, the mid-span, where the slope is singular, in theory. DL_4 stands for the case corresponding to an ordinary section on the beam. DL_4 and DL_6 were calculated by

$$DL_4 = \frac{\frac{D(x_4)-D(x_3)}{\Delta x_{43}}}{\frac{D(x_6)-D(x_4)}{\Delta x_{64}}} = \frac{2[D(x_4)-D(x_3)]}{D(x_6)-D(x_4)} \qquad DL_6 = \frac{D(x_6)-D(x_4)}{2[D(x_7)-D(x_6)]}$$

As shown in Fig. 10, DL_6 differs from DL_4 and DL_7 in three aspects. Firstly, the plus/minus sign of DL_6 changes immediately at the instant of forming the hinge fully, as also predicted in Panel c) in Fig. 4. Secondly, the absolute magnitude of DL_6 is always larger than 2.75 throughout the test, however, most of the values of DL_4 and DL_7 are far smaller than 2.0. For example, when $P = 65$ kN, DL_6 is 3.8125, whereas DL_4 and DL_7 equal 1.7483 and −0.4022, respectively. Finally, compared with DL_6, the values of DL_4 and DL_7 vary differently, as shown in the right panel. Keeping its plus sign, DL_4 decreases gradually to a value of unity. At the mid-span, the sign of DL_7 changes, from the minus to plus; its value firstly decreases to a value of zero, showing the nature of DL_7, a singularity from its definition. After that, the index approaches to unity, meaning a hinge was forming elsewhere. The indices corresponding to the damaged, virgin and mid-span sections vary completely differently in quality and quantity, which matches very well with the previous theoretical prediction in Section 3.4. In conclusion, the slope is able to locate very precisely damage in all developing stages of a defect.

5.4. Further significance of the mode-specific damage identification strategy

So far, a method and corresponding indices for a specific mode of the RC beams have been developed; however, the underlying idea is applicable to a wider range of structure types and circumstances. Two factors, structural behaviours and the development of damage detection investigations, account for the extensive applicability.

Both the characteristics of structural behaviours and engineering practice give rise to the idea. Civil structures can fail in a huge number of modes; however, only a few have high occurrence probabilities [30]; more importantly, these modes contribute to the majority of structural failure probability. In fact, designers and engineers facilitate this predominance deliberately. Namely, they give a higher priority to these modes due to the characteristics of structural behaviour and engineering necessity which have been analysed in Section 2.2. Meanwhile, some modes could cause unaffordable consequences [26], e.g., a massive loss of lives and property. Compared with others, both types of modes deserve more attention. Correspondingly, covering these modes can greatly maximise the safety of the structures and minimise the possible loss due to the failure of the constructions. In conclusion, developing

mode-specific damage identification methods for each important mode is technically essential.

From the perspective of researching methodology, developing mode-specific damage detection methods is necessary. Generally speaking, researchers can learn a lot from the studying philosophy in medical science. Diseases are divided into a great amount of categories and each type of common but critical illness is investigated separately. The damage identification research can take a similar strategy. Namely, all damage scenarios of a particular type of structures are classified according to the occurrence probability and failure consequence, and then the significant ones are covered with corresponding mode-oriented techniques. Herein, the main failure modes or undesirable modes serve as the counterparts of the major illness types in the medical science. More specifically, the mode-specific DI research is more deterministic and easier. Since the behaviour of structures following a particular damage pattern is clearer and more deterministic, the strategy allows researchers to identify damage successfully, with higher effectiveness and less hardness. In fact, a similar mode-oriented NDT idea has been applied in such as Acoustic Emission (AE) studies [42] for decades. In conclusion, developing mode-oriented damage identification methods is suitable and essential for different kinds of civil structures.

6. Conclusions

The fundamental purpose of this research was to suggest a new strategy – studying damage detection methods specific to probabilistically dominant failure modes. The strategy had yielded accurate results in experiments on reinforced concrete (RC) beams. The major conclusions are summarized as follows.

- Among all modes, several occur far more frequently than the rest. For example, in the experiments, when loads were 50 kN, the probability of the flexural failure mode was at least five orders of magnitude greater than those of the others.
- The overwhelming predominance of these modes, to a great extent, results from structural design considerations.
- Hence, developing damage identification techniques just applied to structures which fail in probabilistically dominant modes can greatly enhance their effectiveness, specificity and efficiency.
- In theoretical analysis, simply supported beams failed in the flexural mode demonstrated a unique, interesting characteristic – linearized deflected curves; there was a relation between the damage and the characteristic, Eqs. (5) and (8). More importantly, the damage location and severity indices (Eqs. (13) and (14)) were defined by quantifying the characteristic mathematically.
- The results from the experiments showed that all RC beams failed in the flexural mode and demonstrated the linearized deflection curve feature (Figs. 6–8); that there was a strong correlation between the damage state and the severity index (Fig. 9); that the location index exhibited distinctively different varying patterns at the damaged or intact positions (Fig. 10).

Acknowledgements

This work was funded by Research Project of Science and Technology of Chongqing Education Committee (KJ130426), National Natural Science Foundation of China (51425801, 51478071 and 51508058). The authors thank the anonymous reviewer who demonstrated the true understanding of the academic publication and provided constructive comments that helped in further revising the manuscript. The authors also highly appreciate Prof. Mike POMFRET, Department of Civil and Environmental Engineering, School of Engineering, The HongKong University of Science and Technology, for careful proofreading.

References

[1] D. Dessi, G. Camerlengo, Damage identification techniques via modal curvature analysis: overview and comparison, Mech. Syst. Signal Process. 52 (2015) 181–205.
[2] V. Janapati, F. Kopsaftopoulos, F. Li, S.J. Lee, F.-K. Chang, Damage detection sensitivity characterization of acousto-ultrasound-based structural health monitoring techniques, Struct. Health Monit. 15 (2) (2016) 143–161.
[3] S. Kim, S. Pakzad, D. Culler, J. Demmel, G. Fenves, S. Glaser, et al., Health monitoring of civil infrastructures using wireless sensor networks, in: 2007 6th International Symposium on Information Processing in Sensor Networks, IEEE, 2007, pp. 254–263.
[4] S. Jang, H. Jo, S. Cho, K. Mechitov, J.A. Rice, S.-H. Sim, et al., Structural health monitoring of a cable-stayed bridge using smart sensor technology: deployment and evaluation, Smart Struct. Syst. 6 (5–6) (2010) 439–459.
[5] C.D. Zhang, Y.L. Xu, Structural damage identification via multi-type sensors and response reconstruction, Struct. Health Monit. (2016).
[6] H. Sohn, C.R. Farrar, F.M. Hemez, D.D. Shunk, D.W. Stinemates, B.R. Nadler, et al., A Review of Structural Health Monitoring Literature: 1996–2001, Los Alamos National Laboratory Los Alamos, NM, 2004.
[7] P.C. Chang, A. Flatau, S. Liu, Review paper: health monitoring of civil infrastructure, Struct. Health Monit. 2 (3) (2003) 257–267.
[8] S.W. Doebling, C.R. Farrar, M.B. Prime, D.W. Shevitz, Damage Identification and Health Monitoring of Structural and Mechanical Systems From Changes in Their Vibration Characteristics: A Literature Review, Los Alamos National Lab, NM (United States), 1996.
[9] C.R. Farrar, S.W. Doebling, An overview of modal-based damage identification methods, in: Proceedings of DAMAS Conference, Citeseer, 1997, pp. 269–278.
[10] H. Chen, M. Kurt, Y.S. Lee, D.M. McFarland, L.A. Bergman, A.F. Vakakis, Experimental system identification of the dynamics of a vibro-impact beam with a view towards structural health monitoring and damage detection, Mech. Syst. Signal Process. 46 (1) (2014) 91–113.
[11] Z. Ismail, H. Abdul Razak, A.G. Abdul Rahman, Determination of damage location in RC beams using mode shape derivatives, Eng. Struct. 28 (11) (2006) 1566–1573.
[12] T.M. Whalen, The behavior of higher order mode shape derivatives in damaged, beam-like structures, J. Sound Vib. 309 (3–5) (2008) 426–464.
[13] F. Abbassi, T. Belhadj, S. Mistou, A. Zghal, Parameter identification of a mechanical ductile damage using Artificial Neural Networks in sheet metal forming, Mater. Des. 45 (2013) 605–615.
[14] R. Yao, S.N. Pakzad, Autoregressive statistical pattern recognition algorithms for damage detection in civil structures, Mech. Syst. Signal Process. 31 (2012) 355–368.
[15] A. Kunwar, R. Jha, M. Whelan, K. Janoyan, Damage detection in an experimental bridge model using Hilbert-Huang transform of transient vibrations, Struct. Control Health Monit. 20 (1) (2013) 1–15.
[16] S.S. Patel, A.P. Chourasia, S.K. Panigrahi, J. Parashar, N. Parvez, M. Kumar, Damage identification of RC structures using wavelet transformation, Procedia Eng. 144 (2016) 336–342.
[17] D.L. Hunt, S.P. Weiss, W.M. West, T.A. Dunlap, S. Freesmeyer, Development and implementation of a shuttle modal inspection system, in: Proceedings of the 8th International Modal Analysis Conference, Kissimmee, FL, 1990. pp. 919–925.
[18] J.M. e Silva, Machinery vibration measurements and analysis, in: Vibration and Wear in High Speed Rotating Machinery, Springer, 1990, pp. 221–239.
[19] W. Weijtjens, T. Verbelen, G. De Sitter, C. Devriendt, Foundation structural health monitoring of an offshore wind turbine—a full-scale case study, Struct. Health Monit. 1–14 (2015).
[20] P.F. Viero, N. Roitman, Application of some damage identification methods in offshore platforms, Mar. Struct. 12 (2) (1999) 107–126.
[21] K.-C. Chang, C.-W. Kim, Modal-parameter identification and vibration-based damage detection of a damaged steel truss bridge, Eng. Struct. 122 (2016) 156–173.
[22] R.V. Farahani, D. Penumadu, Damage identification of a full-scale five-girder bridge using time-series analysis of vibration data, Eng. Struct. 115 (2016) 129–139.
[23] P.J. Vardanega, G.T. Webb, P.R.A. Fidler, C.R. Middleton, Assessing the potential value of bridge monitoring systems, Proc. Inst. Civ. Eng. Bridge Eng. 169 (2) (2016) 126–138.
[24] W. Fan, P. Qiao, Vibration-based damage identification methods: a review and comparative study, Struct. Health Monit. 10 (1) (2011) 83–111.
[25] C.Y. Ji, H.Z. Xue, X.H. Shi, O. Gaidai, Experimental and numerical study on collapse of aged jacket platforms caused by corrosion or fatigue cracking, Eng. Struct. 112 (2016) 14–22.
[26] A. Aktan, F. Catbas, K. Grimmelsman, C. Tsikos, Issues in infrastructure health monitoring for management, J. Eng. Mech. 126 (7) (2000) 711–724.
[27] A. Aktan, C. Tsikos, F. Catbas, K. Grimmelsman, R. Barrish, Challenges and opportunities in bridge health monitoring, in: Proceedings of 2nd Int Workshop on Structural Health Monitoring, 1999, pp. 461–473.

[28] S. Chase, Dynamics and field testing of bridges in the new millennium: a look forward, in: A White Paper prepared for Transportation Research Board Technical Committee A2C05 on Dynamics and Field Testing of Bridges, 1999.
[29] P.C. Das, New developments in bridge management methodology, Struct. Eng. Int. 8 (4) (1998) 299–302.
[30] D.-S. Kim, S.-Y. Ok, J. Song, H.-M. Koh, System reliability analysis using dominant failure modes identified by selective searching technique, Reliab. Eng. Syst. Saf. 119 (2013) 316–331.
[31] M.R. Gorman, Reliability of Structural System, Civil Engineering Dept. Case Western Reserve University, Cleveland, Ohio, U.S.A., 1979.
[32] Y. Feng, C. Dong, A method for identifying significant failure modes of a structure system, Acta Aeronautica ET Astronautica Sinica 12 (9) (1991) 537–541.
[33] Committee A, Institute AC, Standardization IOf. Building Code Requirements for Structural Concrete (ACI 318–08) and Commentary, American Concrete Institute, 2008.
[34] H. Rusch, Researches toward a general flexural theory for structural concrete, J. Am. Concr. Inst. 57 (1) (1960) 1–28.
[35] C.S. Whitney, Design of reinforced concrete members under flexure or combined flexure and direct compression, J. Proc. (1937) 483–498.
[36] J.R. Janney, E. Hognestad, D. McHenry, Ultimate Flexural Strength of Prestressed and Conventionally Reinforced Concrete Beams, Portland Cement Association, Research and Development Laboratories, 1956.
[37] CCCC Highway Consultants Co. L., Code for Design of Highway Reinforced Concrete Prestressed Concrete Bridges and Culverts (JTG D62-2012), China Communications Press, Beijing, China, 2012.
[38] de Normalisation CE. Design of Concrete Structures—Part 1–1: General Rules and Rules for Buildings. Eurocode 2, EN 1992-1-1, 2004, E2004.
[39] M.I. Friswell, J.E. Penny, Crack modeling for structural health monitoring, Struct. Health Monit. 1 (2) (2002) 139–148.
[40] A. Teughels, G. De Roeck, Structural damage identification of the highway bridge Z24 by FE model updating, J. Sound Vib. 278 (3) (2004) 589–610.
[41] R.W. Clough, J. Penzien, Dynamics of structures, 2003, p. 180.
[42] D. Crivelli, M. Guagliano, M. Eaton, M. Pearson, S. Al-Jumaili, K. Holford, et al., Localisation and identification of fatigue matrix cracking and delamination in a carbon fibre panel by acoustic emission, Compos. B Eng. 74 (2015) 1–12.